Stability Analysis of Nonlinear Power Electronic Systems Utilizing Periodicity and Introducing Auxiliary State Vector

Octavian Dranga, Balázs Buti, István Nagy, *Fellow, IEEE*, and Hirohito Funato, *Member, IEEE*

***Abstract*—Variable-structure piecewise-linear nonlinear dynamic feedback systems emerge frequently in power electronics. This paper is concerned with the stability analysis of these systems. Although it applies the usual well-known and widely used approach, namely, the eigenvalues of the Jacobian matrix of the Poincaré map function belonging to a fixed point of the system to ascertain the stability, this paper offers two contributions for simplification as well that utilize the periodicity of the structure or configuration sequence and apply an alternative simpler and faster method for the determination of the Jacobian matrix. The new method works with differences of state variables rather than derivatives of the Poincaré map function (PMF) and offers geometric interpretations for each step. The determination of the derivates of PMF is not needed. A key element is the introduction of the so-called auxiliary state vector for preserving the switching instant belonging to the periodic steady-state unchanged even after the small deviations of the system orbit around the fixed point. In addition, the application of the method is illustrated on a resonant dc–dc buck converter.**

***Index Terms*—DC–DC power conversion, nonlinear systems, stability, variable-structure systems.**

I. Introduction

LARGE numbers of converters in power electronics belong to the variable-structure, piecewise-linear nonlinear dynamic feedback systems. They change their structure and their configuration after each switching, and the sequence of structures succeeds each other periodically in the periodic steady state. Each structure of the converters can be modeled with good approximation by linear circuitry, and therefore they are piecewise linear. The overall systems are nonlinear due to the dependence of switching instants on state variables stemming from the feedback control loop and due to saturation or other nonlinearities.

The paper is concerned with the stability of such systems. Besides the periodicity of the configuration sequence, the switchings have to be controlled by pulse width modulation (PWM) in the system. It must be emphasized that the stability study used in the paper is based on the well-known and widely applied approach in which the eigenvalues of the Jacobian matrix of the Poincaré map function are determined at a fixed point of the system [1]–[12]. From a physical viewpoint, it is equivalent to study the behavior of the trajectory of the system in state space when it is forced to leave its periodic steady-state trajectory to a new orbit by a small deviation from the original trajectory.

This paper offers new contributions, to the best of the authors' knowledge, to the usual stability analysis in two points. The first point is utilizing the periodicity of the structure sequence and introducing subperiods. State equations have to be derived only for one subperiod, which reduces the number of state equations needed for the stability analysis. We do not consider it as major contribution but it can be very useful. This method has already been used once [13], but it has not been introduced in a generic way. Second, and most important, we determine the Jacobian matrix by using the small differences of state vectors compared to their steady-state values at the start and end of subperiods and at the switching instant. There is no need to determine the derivates of the Poincaré map function at the fixed point. The Jacobian matrix is obtained directly from the relations among the small differences of state vectors. In addition, all steps are interpreted graphically. Consequently, this method offers an alternative way to derive the Jacobian matrix or, which is more significant, a simpler and faster way to determine it. The key element of this method is the introduction of the auxiliary state vector for preserving constant switching instants for the switchings depending on state variables even after the small excursion of the state variables from the steady state, although they vary in small extent.

The method is described in a generic way in Sections II–V. The application of the method is illustrated with a dual channel dc–dc resonant converter in Sections VI and VII and the Appendix).

II. Power Electronic Circuits as Variable-Structure Systems

Fig. 1(a) presents the simplified block diagram of the type of systems discussed. The controlled object is the variable-struc-

Manuscript received March 19, 2003, revised August 2, 2004. This work was supported by the Hungarian Research Fund under Grant OTKA TO34654, Grant OTKA TO34630, and Grant OTKA TO46240, and by the Control Research Group of the Hungarian Academy of Science. This paper was recommended by Associate Editor M. K. Kazimierczuk.

O. Dranga is with the Department of Electronic and Information Engineering, The Hong Kong Polytechnic University, Kowloon, Hong Kong (e-mail: oktav@elektro.get.bme.hu).

B. Buti is with the Department of Automation and Applied Informatics, Budapest University of Technology and Economics, H-1111 Budapest, Hungary (e-mail: but@elektro.get.bme.hu).

I. Nagy is with the Department of Automation and Applied Informatics, Budapest University of Technology and Economics, H-1111 Budapest, Hungary, and also with the Computer and Automation Institute, Hungarian Academy of Sciences, H-1111 Budapest, Hungary (e-mail: nagy@elektro.get.bme.hu).

H. Funato is with the Department of Electrical and Electronic Engineering, Utsunomiya University, Utsunomiya 321-8585, Japan (e-mail: funato@cc.utsunomiya-u.ac.jp).

Digital Object Identifier 10.1109/TCSI.2004.840102

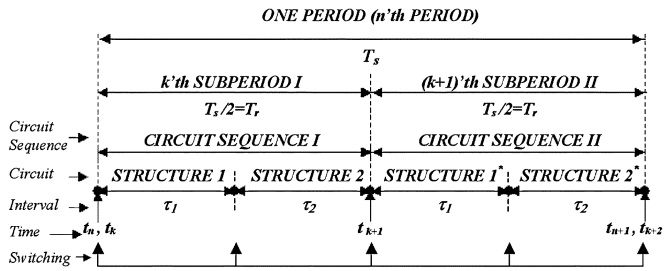

Fig. 1. Time sequence of structure changes in the periodic steady state.

ture power part with controlled switches, incorporating periodically changing subcircuits, which are cyclically turned on and off. The output voltage v_o is controlled by PWM. The carrier signal $v_{\rm carrier}$ can be, e.g., a ramp function (saw-tooth waveform) [see Fig. 1(b)]. The output signal of the controller $v_{\rm con}$ is compared to the carrier signal $v_{\rm carrier}$. The state of the controlled switches depends on the sign of $e = v_{\rm con} - v_{\rm carrier}$. Having only one switch in the controlled object in the simplest case, the period of the ramp signal T_r and the period of the state variables T_s are equal to each other as in a hard-switched buck, boost and buck, and boost dc–dc converters [Fig. 1(b)]. When two controlled switches are in the controlled object and they are turned on and off alternately, as we will see in our example, $T_s = 2T_r$. Switching occurs in the controlled object at each transition in $v_{\rm switch}$ from 0 to 1 or *vice-versa*. Two kinds of switching take place: asynchronous A-switching and synchronous S-switching [Fig. 1(b)].

In order to make as clear and simple as possible the description of the alternative method of deriving the Jacobian matrix within the frame of stability study, which is the main target of the paper, the simple proportional controller

$$v_{\rm con} = K_v(V_{\rm ref} - v_o) \tag{1}$$

will be assumed.

The controlled object is a variable-structure piecewise-linear system. After each switch, another linear circuit emerges and the sequence of linear circuits is repeated in the next T_s period [13].

Fig. 2 shows the time sequence of structure changes within one T_s period as a simple example. The dual-channel resonant dc–dc converter has, in fact, this sequence of structure changes, as will be shown later on. Here, one period has two subperiods $p = 2$, where p is the number of subperiods in one T_s period and each subperiod consists of two linear circuits called structures $(s = 2)$. Suffixes $n = 1, 2, \ldots$, and $k = 1, 2, \ldots$ are used for counting the number of periods and subperiods $(k = pn)$ starting from the beginning of the transient process, respectively.

Building up a linear circuit model on the basis of the actual configuration of the power electronics converter corresponding to the actual state of the switches, the model is the same for structure 1 in subperiod I and for structure 1* in subperiod II. The same statement holds for structures 2 and 2*. Therefore, the sequence of models repeats itself in each subperiod. At the same time, the actual energy storage components, resistances, switches, and the associated state variables belonging to the

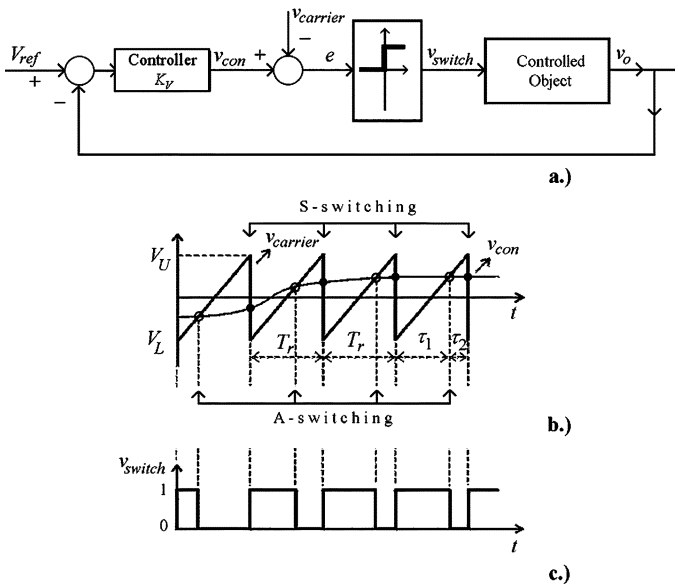

Fig. 2. (a) Block diagram of the variable-structure piecewise-linear feedback system controlled by PWM. (b) Carrier signal is a saw-tooth wave. (c) Switching signal $v_{\rm switch}$.

same successive structures (e.g., structures 1 and 1*) might be partially or entirely different.

Due to the identical structures (1 and 1* as well as 2 and 2*) in the two subperiods, the state equations in the two τ_1 intervals (and in the two τ_2 intervals) have the same mathematical forms. The state variables can be different in the same places of the equations, but the values of the parameters are the same due to symmetry. The identity of the form of state equations makes it possible to calculate the dynamic processes in subperiod II and, in general, in subperiod p by using only the state equations of subperiod I. The state vector $\underline{x}_e$ at the end of subperiod I has to be transformed back in an appropriate way to the starting state vector $\underline{x}_s$ of subperiod I (Section III). The state variables of subperiod I are used for the calculation of state variables of subperiod II. Their identification with the actual state variables of subperiod II that they represent can easily be done. Applying only the state equations of subperiod I together with the back transformation, the whole period can be treated.

The method described in the paper can be extended for systems with a more sophisticated structure sequence if otherwise the systems meet the other restrictions described.

III. Mathematical Background

Everything in this section is well known except the concept of back transformation. The aim of this section is mainly the introduction of notations used later on.

The variable-structure system shown in Fig. 1(a) is nonautonomous due to signal $v_{\rm carrier}$ [1]–[3]. The controlled object within structures 1 and 2 is linear, and it can be described by the coupled first-order linear differential equation system or state equation

$$\underline{v}_i = \frac{d\underline{x}_i}{dt} = \underline{A}_i\underline{x}_i + \underline{B}_i\underline{u}_i \tag{2}$$

in the interval $\tau_i, i = 1,2\ldots$ (Fig. 2) where $\underline{v}_i$ is the velocity vector, $\underline{x}_i$ is the state vector, and $\underline{u}_i$ is the excitation vector. Matrices $\underline{A}_i$ and $\underline{B}_i$ depend on the configuration and parameters of the respective structure in the controlled object. At the switching instant, the velocity vector is suddenly changed, e.g., at $t_k + \tau_1$ (Fig. 2) as follows:

$$\Delta \underline{v}_{12} = \underline{v}_{2,s} - \underline{v}_{1,e} \tag{3}$$

where suffixes s and e stand for start and end, respectively. $\Delta \underline{v}_{12}$ acts upon the system as a "force," and the direction of the system trajectory is abruptly varied in the state space.

The solution of (2) is well known, and its expression is

$$\underline{x}(\tau) = \underline{x}_p + \underline{W}(\tau)[\underline{x}(0) - \underline{x}_p] \tag{4}$$

where suffix i has been dropped, and τ is the time elapsed from the switching instant. The weighting matrix

$$\underline{W}(\tau) = e^{\underline{A}\tau} \tag{5}$$

and the particular solution from (2) is $\underline{x}_p = -\underline{A}^{-1}\underline{B}\,\underline{u}$

Having two structures within a subperiod (Fig. 2), (4) has to be applied twice, always with the respective values pertaining to the actual structure.

In the steady state, the periodicity or transfer matrix $\underline{T}$ connects the values of the state vector at the start and the end of the subperiod I

$$\underline{x}_{k2,e} = \underline{T}\,\underline{x}_{k1,s} \tag{6}$$

or

$$\underline{x}_{k1,s} = \underline{x}_{(k+1)1,s} = \underline{T}^{-1}\underline{x}_{k2,e} \tag{7}$$

where the elements in matrix $\underline{T}$ are $1, -1$, or 0 (cf. the example in Section VI and in the Appendix) and $\underline{x}_{k1,s} = \underline{x}(t_k); \underline{x}_{k2,e} = \underline{x}(t_{k+1})$ (Fig. 2). Suffixes 1 and 2 stand for structures 1 and 2, respectively. Knowing the operation of the respective power electronics configuration, the determination of $\underline{T}$ is a simple task, as will be seen later on. Equation (7) can be interpreted as follows. After calculating $\underline{x}_{k2,e}$, the operation $\underline{T}^{-1}\underline{x}_{k2,e}$ is a back transformation of $\underline{x}_{k2,e}$ to the start of subperiod I in order to apply $\underline{x}_{k1,s}$ as the initial value in the same state equations (that were used in subperiod I) for the calculations of the state variables in subperiod II.

The interval τ_1 (and $\tau_2 = T_r - \tau_1$) can be determined from the rule of PWM switching (1) and Fig. 1(b)

$$\begin{aligned} e(\tau_1) &= v_{\text{con}}(\tau_1) - v_{\text{carrier}}(\tau_1) \\ &= K_v[V_{\text{ref}} - v_0(\tau_1)] - v_{\text{carrier}}(\tau_1) = 0. \end{aligned} \tag{8}$$

Although the equations of the controlled object (2) and (7) are linear, the last relation (8) is nonlinear due to the dependence of τ_1 on the state variable v_0 [and because v_{con} can be higher than V_U or lower than V_L; see Fig. 1(b)], resulting in no switching in one or more consecutive T_r subperiods). In general, the calculation of τ_1 from the nonlinear equation leads to an iteration procedure.

IV. Small Changes Around the Periodic State and Auxiliary State Vector

The system trajectory keeps circulating along the same closed loop in state space in the periodic state. As an example, Fig. 3 shows the trajectory of state vector $\underline{x}$ and its start $(\underline{x}_s)$ and end $(\underline{x}_e)$ positions in subperiod I in the steady state in three-dimensional (3-D) state space (heavy solid line). In the periodic steady state, the trajectory pierces through the Poincaré plane at point D_s where the state vector is $\underline{x}_s$, which is the fixed point. After subperiod I, the state vector is $\underline{x}_e$ (point D_e). Transforming $\underline{x}_e$ back to the start of subperiod I by matrix $\underline{T}^{-1}$, the original state vector $\underline{x}_s$ is reobtained: $\underline{x}_s = \underline{T}^{-1}\,\underline{x}_e$ [(7)]. The system trajectory starts from the fixed point again.

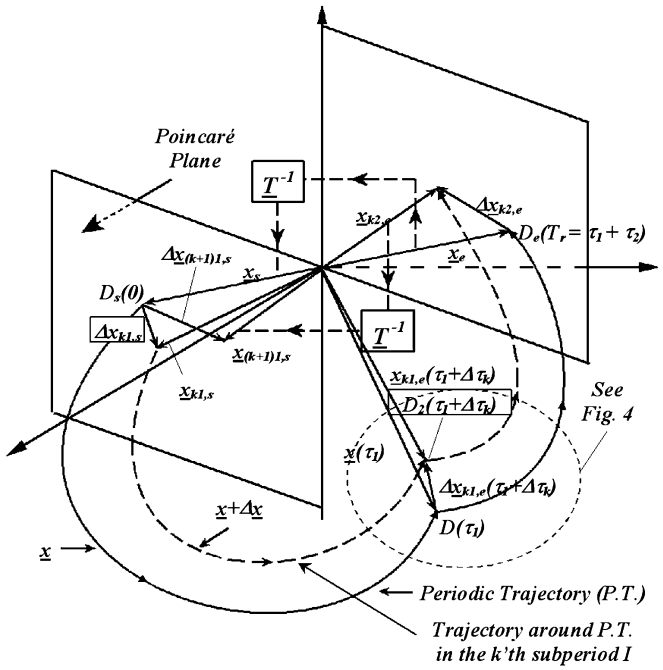

Fig. 3. Back transformation of $\underline{x}_e$ to the start of the next subperiod I. Trajectory in the steady state (heavy solid line). Trajectory after small deviation from the steady state (dashed line).

Due to a small deviation of the trajectory from point D_s, the small change in the state vector at the start of the kth subperiod I is $\Delta \underline{x}_{k1,s}$ and the state vector is $\underline{x}_{k1,s}$ in Fig. 3. At the end of the kth subperiod I, the state vector is $\underline{x}_{k2,e}$. Suffixes 1 and 2 refer to structures 1 and 2, respectively (Fig. 2). Transforming back $\underline{x}_{k2,e}$ to the start of the $(k+1)$th subperiod, we obtain

$$\underline{x}_{(k+1)1,s} = {}^{-}\underline{T}^{-1}\underline{x}_{k2,e}. \tag{9}$$

As a result of the small deviation around the periodic state, $T_r = \tau_1 + \tau_2$ remains unchanged but, in general, τ_1 is changed in the kth subperiod by $\Delta\tau_k$ due to its dependence on the changing state variable v_0 [Fig. 1(b) and (8)]. $\Delta\tau_k$ varies from subperiod to subperiod. (It is assumed that $V_L \le v_{\text{con}} \le V_U$ holds.) The stability calculation or, more precisely, the calculation of the Jacobian matrix is greatly simplified by introducing an *auxiliary state vector* $\underline{x}_{k2,s}\,(\tau_1)$ at the structure change from 1 to 2 at τ_1 (Fig. 2) and its *change* $\Delta \underline{x}_{k2,s}\,(\tau_1)$ in place of the actual state vector change $\Delta \underline{x}_{k1,e}(\tau_1 + \Delta\tau_k)$ (Fig. 4). This permits us to take into account the effect of the $\Delta\tau_k$ change but at the same time keep τ_1 and, consequently, τ_2 unchanged. The rewards of this method are as follows.

1) To determine the Jacobian matrix, we do not have to calculate the derivatives of the Poincaré map function (PMF).

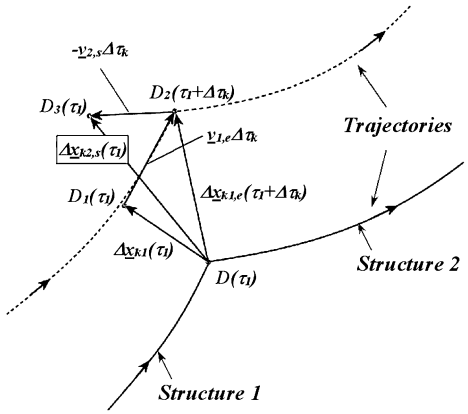

Fig. 4. Auxiliary state vector change $\Delta\underline{x}_{2,s}(\tau_1)$ (see Fig. 3).

2) The Jacobian matrix is directly obtained from the relations among the small changes of the state vectors written on the basis of Figs. 3 and 4 and from (8) rewritten for small changes. The equations have graphical interpretation.
3) Weighting matrices $\underline{W}_1$ (τ_1) and $\underline{W}_2$ (τ_2) can be applied for small changes as well.

τ_1 has to be calculated by an iteration process only once for the periodic steady state. The description of the iteration process for the calculation of τ_1 is straightforward and beyond the scope of this paper. we refer the reader to [13].

On the basis of (4), the relation between the small changes of the state vector in structures 1 and 2 are as follows (Fig. 4):

$$\Delta\underline{x}_{k1}(\tau_1) = \underline{W}_1(\tau_1)\Delta\underline{x}_{k1,s}(0) = e^{\underline{A}_1\tau_1}\Delta\underline{x}_{k1,s}(0) \quad (10)$$

$$\Delta\underline{x}_{k2,e}(\tau_2) = \underline{W}_2(\tau_2)\Delta\underline{x}_{k2,s}(\tau_1) = e^{\underline{A}_2\tau_2}\Delta\underline{x}_{k2,s}(\tau_1) \quad (11)$$

where $\Delta\underline{x}_{k1}$ is the small change in the state vector at τ_1, that is, in advance by $\Delta\tau_k$ before the end of the kth subperiod I. By knowing structures 1 and 2, we know $\underline{A}_1$ and $\underline{A}_2$; therefore, the determination of $\underline{W}_1(\tau_1)$ and $\underline{W}_2(\tau_2)$ is straightforward.

All small changes are real values, but the fictitious auxiliary state vector change $\Delta\underline{x}_{k2,s}(\tau_1)$ can be determined from

$$\Delta\underline{x}_{k2,s}(\tau_1) = \underline{M}\Delta\underline{x}_{k1}(\tau_1) \quad (12)$$

where matrix $\underline{M}$ can be derived from Fig. 4, as will be shown later.

The starting point is the periodic trajectory or limit cycle of the system. A small section of the trajectory in the neighborhood of the switching from structure 1 to structure 2 is shown by the heavy solid line in Fig. 4, which is a blow up around point $D(\tau_1)$ in Fig. 3. The trajectory reaches the switching hypersurface at point D (τ_1) in the periodic steady state where the velocity vector is abruptly changed [(3)]. After deviating the system from its limit cycle by a tiny change, the dashed line illustrates the corresponding section of the new trajectory around point $D_2(\tau_1+\Delta\tau_k)$, where the switching hypersurface is reached by this new trajectory at $\tau_1+\Delta\tau_k$ The "distance" between D_1 and D_2 is $\underline{v}_{1,e}\Delta\tau_k$, where $\underline{v}_{1,e}$ is the velocity vector at point D still in structure 1. The alteration of the state vector on the hypersurface is $\Delta\underline{x}_{k1,e}(\tau_1+\Delta\tau_k)$. After the switching, the velocity vector at the start of structure 2 is $\underline{v}_{2,s}$ at point D. The determination of $\underline{v}_{1,e}$ and $\underline{v}_{2,s}$ will be discussed soon. Due to the linearity of the structures, the new trajectory can be projected "backward in time" from time $(\tau_1+\Delta\tau_k)$ to τ_1. In other words, the trajectory will start from point $D_3(\tau_1)$ rather than point $D_2(\tau_1+\Delta\tau_k)$ by extending the new trajectory at the start of structure 2 toward "negative time" in the direction of the velocity vector $(-\underline{v}_{2,s})$. Point $D_3(\tau_1)$ is reached this way at distance $-\underline{v}_{2,s}\Delta\tau_k$ from D_2 The *auxiliary state vector change* $\Delta\underline{x}_{k2,s}(\tau_1)$ is obtained between points D_3 and D. This mathematical abstraction is useful since, by applying $\Delta\underline{x}_{k2,s}(\tau_1)$ in place of $\Delta\underline{x}_{k1,e}(\tau_1+\Delta\tau_k)$, the trajectory will start in structure 2 at the same instant τ_1 as in the case of the periodic trajectory.

Turning to the determination of the relation between the real state vector change $\Delta\underline{x}_{k1}(\tau_1)$ and the auxiliary one $\Delta\underline{x}_{k2,s}(\tau_1)$, the following relationship is obtained from triangles DD_1D_2 and DD_2D_3:

$$\Delta\underline{x}_{k2,s}(\tau_1) = \Delta\underline{x}_{k1}(\tau_1) + (\underline{v}_{1,e} - \underline{v}_{2,s})\cdot\Delta\tau_k. \quad (13)$$

By introducing the *auxiliary state vector* $\underline{x}(\tau_1)+\Delta\underline{x}_{k2,s}(\tau_1)$ directed to point $D_3(\tau_1)$ and the *auxiliary state vector change* $\Delta\underline{x}_{k2,s}(\tau_1)$, the application of τ_1 as the unchanged interval for structure 1 is still permitted in the relations among the small deviations.

V. Determination of the Jacobian Matrix on the Basis of the Auxiliary State Vector

The aim is the determination of $\underline{J}_K$, the Jacobian matrix of the subperiods belonging to the fixed point D_s. The relation among the consecutive small deviations of the state vector $\underline{x}$ around the fixed point D_s is

$$\Delta\underline{x}_{(k+1)1,s} = \underline{J}_K\Delta\underline{x}_{k1,s} = \underline{J}_K^k\Delta\underline{x}_{11,s} \quad (14)$$

where $\Delta\underline{x}_{11,s}$ is the initial deviation of state vector $\underline{x}(k=1)$ at fixed point D_s.

At the start of the $(k+2)$th subperiod, we have

$$\Delta\underline{x}_{(k+2)1,s} = \underline{J}_K\Delta\underline{x}_{(k+1)1,s} = \underline{J}_K^2\Delta\underline{x}_{k1,s} = \underline{J}_N\Delta\underline{x}_{k1,s} \quad (15)$$

where $\underline{J}_N$ is the Jacobian matrix of the whole switching period T_S. Therefore

$$\underline{J}_N = \underline{J}_K^2. \quad (16)$$

The eigenvalues of Jacobian matrix $\underline{J}_N$ equals the square of those of Jacobian matrix $\underline{J}_K$. The stability of the fixed point D_s can be concluded either from $\underline{J}_N$ or $\underline{J}_K$. When the eigenvalues of $\underline{J}_N$ are within the unit circle, those of $\underline{J}_K$ are inside the unit circle as well, and *vice-versa*.

After determining $\Delta\underline{x}_{k1}(\tau_1)$ from (10), the next step is the calculation of the auxiliary state vector change $\Delta\underline{x}_{k2,s}(\tau_1)$ from (12). We have to know matrix $\underline{M}$ at this step. $\underline{M}$ can be derived from (13) if $\Delta\tau_k$ can be expressed by $\Delta\underline{x}_{k1}(\tau_1)$.

To determine $\Delta\tau_k$ with $\Delta\underline{x}_{k1}(\tau_1)$, the rule of PWM switching has to be used [see (8)]. Assuming that the output voltage of the controlled object [Fig. 1(a)] is a state variable, v_0 is one element of state vector $\underline{x}$ and $v_0(\tau_1)$ can be expressed by $\underline{x}(\tau_1)$, that is, $v_0(\tau_1) = \underline{k}^T\ \underline{x}_{1,e}(\tau_1)$ where $\underline{k}^T = [0\ldots1\ldots0]$. All elements

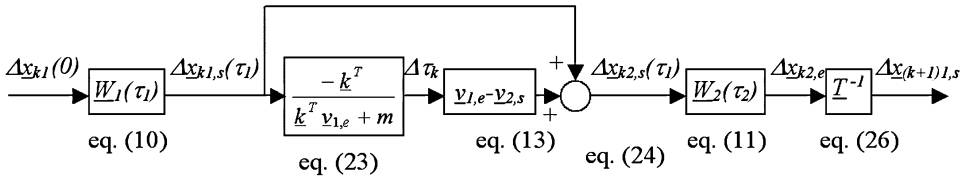

Fig. 5. Calculation sequence of the Jacobian matrix $\underline{J}_K$.

of constant vector $\underline{k}^T$ are zero except one (or two, see later[1]) belonging to v_0. The transposition of vector $\underline{k}$ is denoted by $\underline{k}^T$.

The relation for v_{carrier} is [Fig. 1(b)]

$$v_{\text{carrier}} = V_L + \frac{V_U - V_L}{T_r}\tau = V_L + m\tau. \tag{17}$$

Equation (8) can be rewritten at $\tau = \tau_1$ as

$$e(\tau_1) = 0 = K_v[V_{\text{ref}} - \underline{k}^T\underline{x}(\tau_1)] - V_L - m\tau_1 \tag{18}$$

and at $\tau = \tau_1 + \Delta\tau_k$ as

$$e(\tau_1 + \Delta\tau_k) = 0 = K_v\{V_{\text{ref}} - \underline{k}^T[\underline{x}(\tau_1) + \Delta\underline{x}_{k1,e}(\tau_1 + \Delta\tau_k)]\} - V_L - m(\tau_1 + \Delta\tau_k). \tag{19}$$

Subtracting (19) from (18) yields

$$\underline{k}^T\Delta\underline{x}_{k1,e}(\tau_1 + \Delta\tau_k) + m\Delta\tau_k = 0. \tag{20}$$

From triangle DD_1D_2, we have

$$\Delta\underline{x}_{k1,e}(\tau_1 + \Delta\tau_k) = \Delta\underline{x}_{k1}(\tau_1) + \underline{v}_{1,e}\Delta\tau_k. \tag{21}$$

Substituting (21) into (20) yields

$$\underline{k}^T[\Delta\underline{x}_{k1}(\tau_1) + \underline{v}_{1,e}\Delta\tau_k] + m\Delta\tau_k = 0 \tag{22}$$

and from here

$$\Delta\tau_k = -\frac{\underline{k}^T\Delta\underline{x}_{k1}(\tau_1)}{\underline{k}^T\underline{v}_{1,e} + m}. \tag{23}$$

Substituting $\Delta\tau_k$ from (23) into (13) results in the following relationship for which we are looking:

$$\Delta\underline{x}_{k2,s}(\tau_1) = \left[\underline{I} - \frac{\underline{v}_{1,e} - \underline{v}_{2,s}}{\underline{k}^T \cdot \underline{v}_{1,e} + m} \cdot \underline{k}^T\right] \cdot \Delta\underline{x}_{k1}(\tau_1) = \underline{M}\Delta\underline{x}_{k1}(\tau_1) \tag{24}$$

where $\Delta\underline{x}_{k2,s}(\tau_1)$ is the *auxiliary state vector change* at the start of structure 2 and $\underline{I}$ is the identity or unit matrix. Equation (24) determines matrix $\underline{M}$ introduced in (12). The *auxiliary state vector change* $\Delta\underline{x}_{k2,s}(\tau_1)$ permitting us to calculate with the constant switching interval τ_1 can be determined by matrix $\underline{M}$ from state vector change $\Delta\underline{x}_{k1}(\tau_1)$.

Applying (10)–(12) in cascade for the entire kth subperiod I yields

$$\Delta\underline{x}_{k2,e} = \underline{W}_2(\tau_2)\underline{M}\,\underline{W}_1(\tau_1)\Delta\underline{x}_{k1,s}. \tag{25}$$

[1]In the example, in Section VI $v_o = v_{\text{op}} + v_{\text{on}}$ and both v_{op} and v_{on} are state variables [(A1)].

Note that (25) is the same in each subperiod. Due to the periodicity, $\Delta\underline{x}_{k2,e}$ has to be transformed back to the start of subperiod I [see Figs. 2 and 3 and (9)] to yield

$$\Delta\underline{x}_{(k+1)1,s} = \underline{T}^{-1}\underline{W}_2(\tau_2)\underline{M}\,\underline{W}_1(\tau_1)\Delta\underline{x}_{k1,s} = \underline{T}^{-1}\Delta\underline{x}_{k2,e}. \tag{26}$$

Comparing (14) and (26), the Jacobian matrix is

$$\underline{J}_K = \underline{T}^{-1}\underline{W}_2(\tau_2)\underline{M}\underline{W}_1(\tau_1). \tag{27}$$

A. Speed Vectors

To determine the speed vectors $\underline{v}_{1,e}$ and $\underline{v}_{2,s}$, first we have to know the state vector $\underline{x}_s$ at the fixed point. Assuming that we know $\underline{x}_s$ and applying (4), the state vector at τ_1

$$\underline{x}(\tau_1) = \underline{W}_1(\tau_1)\underline{x}_s + [\underline{W}_1(\tau_1) - \underline{I}]\underline{A}_1^{-1}\underline{B}_1\underline{u}_1 \tag{28}$$

and at the end of subperiod I

$$\underline{x}_e = \underline{W}_2(\tau_2)\underline{x}(\tau_1) \tag{29}$$

where $\underline{u}_2 = 0$ is assumed.

In steady state

$$\underline{x}_s = \underline{T}^{-1}\underline{x}_e. \tag{30}$$

From the last equations, we have

$$\underline{x}_s = [\underline{T} - \underline{W}_2(\tau_2)\underline{W}_1(\tau_1)]^{-1}\underline{W}_2(\tau_2)[\underline{W}_1(\tau_1) - \underline{I}]\underline{A}_1^{-1}\underline{B}_1\underline{u}_1. \tag{31}$$

By knowing $\underline{x}(\tau_1) = \underline{x}_{1,e}(\tau_1)$ from (28), the velocity vector from (2) yields

$$\underline{v}_{1,e} = \left(\frac{dx_1}{dt}\right)_{\tau_1} = \underline{A}_1\underline{x}(\tau_1) + \underline{B}_1\underline{u}_1 \tag{32}$$

$$\underline{v}_{2,s} = \left(\frac{dx_2}{dt}\right)_{\tau_1} = \underline{A}_2\underline{x}(\tau_1). \tag{33}$$

On the basis of (28)–(30), the PMF is

$$\underline{x}_{k+1,s} = \underline{P}_k(\underline{x}_{k,s}) = \underline{T}^{-1}\underline{W}_2(\tau_2)\left[\underline{W}_1(\tau_1)\underline{x}_{k,s} + (\underline{W}_1(\tau_1) - \underline{I})\underline{A}_1^{-1}\underline{B}_1\underline{u}_1\right]. \tag{34}$$

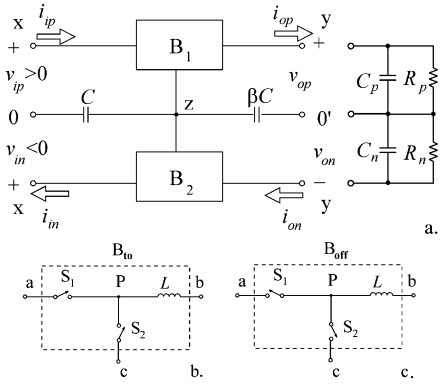

Fig. 6. (a) General configuration of the converters. (b), (c) Basic building blocks.

TABLE I
SETUP OF THE CONVERTERS

	x	y	z	B_1	B_2
Buck	a	b	c	B_{to}	B_{off}
B&B	c	a	b	B_{to}	B_{off}
Boost	b	c	a	B_{off}	B_{to}

We did not apply the derivative of $\underline{P}_k$ in the derivation of the Jacobian matrix $\underline{J}_K$.

Now that we know all terms in matrix $\underline{J}_K$, its eigenvalues and, similarly, the eigenvalues of the Jacobian matrix J_N can be calculated, that is, the stability of the periodic state can be ascertained.

Fig. 5 summarizes the calculation sequence of the Jacobian matrix $\underline{J}_K$. It can be concluded that the derivatives of the PMF are not needed for the determination of the Jacobian matrix. Reference [13] discusses the determination of the Jacobian matrix for exactly the same type of power electronics systems using the traditional approach, that is, from the derivatives of the PMF. The comparison shows clearly how much simpler and faster the direct method is than the traditional one (see [13, Secs. VI-B and C] and compare it with Section V of this paper); of course, the results are the same. Compare (24) and (27) to [13, eqs. (37) and (38)].

VI. EXAMPLE: DC–DC CONVERTER CONFIGURATION AND OPERATION

As an example, a dual-channel resonant buck configuration is chosen. The converter is a member of a converter family. A comprehensive study of the family has been published earlier [26]. Here, only a short description of the configurations and the operation of the members of the family is given. It was previously studied in [13] and [25] by using the traditional approach for determining the Jacobian matrix.

The general configuration of the family shown in Fig. 6(a) has a positive (suffix p) and a negative (suffix n) channel, two switched capacitors $C, \beta C$, two basic building blocks B_1 and B_2, two filter capacitors C_p and C_n, and the loads R_p and R_n. Suffixes i and o refer to input and output, respectively. The configurations of the basic building blocks can be

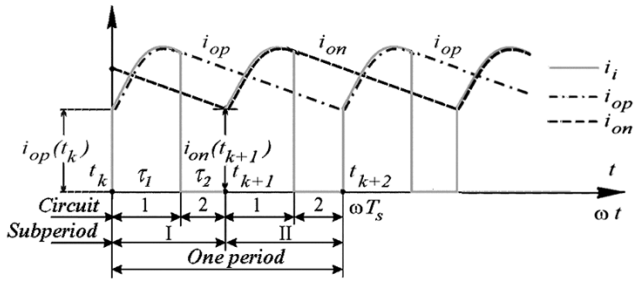

Fig. 7. Time functions of input and output (inductor) currents ($\omega = 1/\sqrt{LC}$).

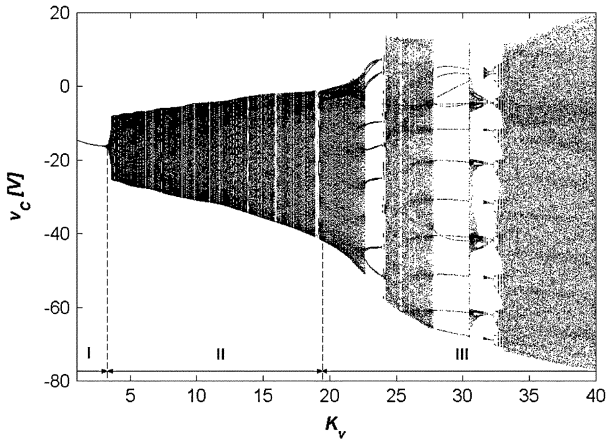

Fig. 8. Bifurcation diagram: I—periodic range; II—quasi-periodic and subharmonic range; III—chaotic and subharmonic range.

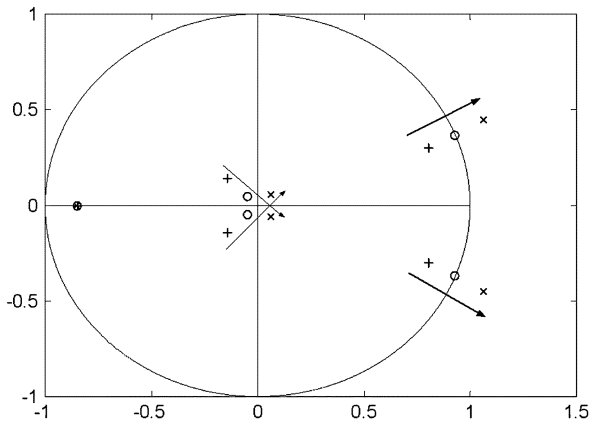

Fig. 9. Loci of eigenvalues ($R = 6\ \Omega$) as the controller gain K_v varies. Arrows indicate increasing gain.

either B_{to} or B_{off} with two controlled switches S_1 and S_2 and inductance L [see Fig. 6(b) and (c)]. The controlled switches (IGBTs, MOSFETs, or other switches) conduct current in the direction of the arrow.

Using the general configuration, any one of the buck, buck and boost, or boost converters can be built by connecting the a, b, and c terminals of the basic building blocks in the way shown in Table I to terminals x, y, and z.

We have selected as an example the buck converter when terminals z and 0' are shorted ($\beta = 0$) and assumed complete symmetry both in the setup ($C_p = C_n = C_o, R_p = R_n = R$) and in the supply ($v_{ip} = -v_{\text{in}} = V_i = \text{const}$ and smooth).

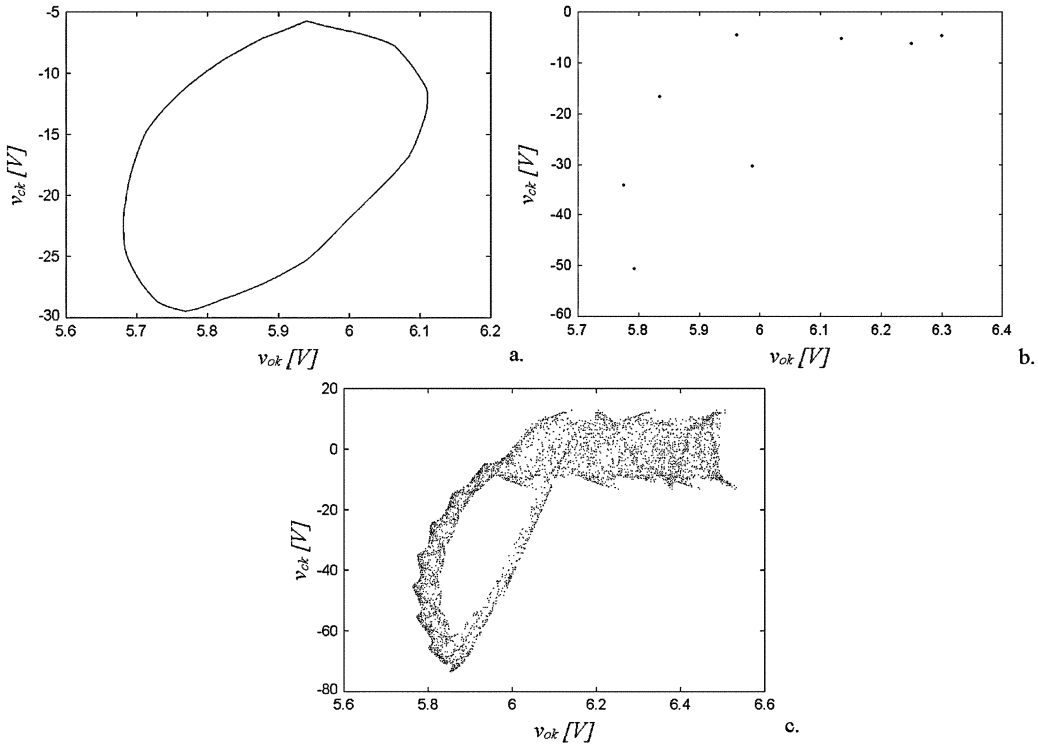

Fig. 10. Stroboscopic maps in (a) quasi-periodic ($K_v = 8$), (b) subharmonic ($K_v = 23$), and (c) chaotic ($K_v = 35$) operation.

A. Operation

Symmetrical, periodic, steady-state operation is summarized. The controlled switches within one channel are always in complementary states (that is, when S_1 is on, S_2 is off, and *vice-versa*). The commutation times between S_1 and S_2 are neglected. The operation of the positive channel is described.

By turning on switch S_1, a sinusoidal current pulse $i_{ip} = i_{\rm op}$ is developed from t_k to $t_k + \tau_1$ in circuit $S_1, L_p, v_{\rm op}, C$, and v_{ip} (Fig. 7). The capacitor voltage v_c swings from V_{cn} to $V_{cp}(V_{cn} < 0)$. By turning on switch S_2 at $t_k + \tau_1$, the choke current $i_{\rm op}$ commutes from S_1 to S_2 and v_L is clamped on V_{cp}. The energy stored in the choke at $t_k + \tau_1$ is depleting in the interval $t_k + \tau_1 < t < t_{k+2} = T_s$. Continuous-conduction mode (CCM) of operation is assumed, that is, the inductor current $i_{\rm op}$ flows continuously ($i_{\rm op} > 0$) (Fig. 7). To give an insight into the operation, first constant and smooth output voltages $v_{\rm op}$ and $v_{\rm on}$ are assumed, although this assumption is dropped in the mathematical description. The inductor current $i_{\rm op}$ decreases in a linear fashion.

The same process takes place at the negative side, resulting in a negative current pulse $i_{\rm on}$ and condenser voltage swing after turning on S_1 in channel n at the beginning of the next half cycle at $T_s/2$ (Fig. 7). (For interested readers, the time functions of $v_{\rm op}, v_{\rm on}$, and v_c can be found in [13, Fig. 2].)

Note that there are two subperiods in one period T_s and each subperiod has two structures (Figs. 2 and 7). Due to the symmetrical setup of the two channels, structures 1 and 2 in the two subperiods are the same, and only the active and passive elements might be different, e.g., in place of S_1, S_2 (in channel p), L_p, and C_p, the corresponding components are S_1, S_2 (in channel n), L_n, and C_n. Similarly, the state variable belonging to the elements might change, e.g., $i_{\rm on}$ replaces $i_{\rm op}$ in the inductor. However, the element and its state variable can be the same in the two subperiods, e.g., switched capacitance C and its state variable v_c.

The state equations for structures 1 and 2 of subperiod I are derived in the Appendix. The result in per unit for structure1 [cf. (A2)] is

$$\frac{d\underline{x}}{dt_r} = \underline{A}_1 \cdot \underline{x} + \underline{B}_1 \tag{35}$$

and for structure 2 [cf. (A4)] is

$$\frac{d\underline{x}}{dt_r} = \underline{A}_2 \cdot \underline{x} \tag{36}$$

where $\underline{x}^T = [x_1 \;\; x_2 \;\; x_3 \;\; x_4 \;\; x_5], x_1 = v_{\rm op}/(V_i/2)$, $x_2 = v_{\rm on}/(V_i/2), x_3 = v_c/(V_i/2), x_4 = Zi_{\rm op}/(V_i/2)$, $x_5 = Zi_{\rm on}/(V_i/2), t_r = t/T_r$, and $Z = \sqrt{L/C}$.

By utilizing the periodicity of the structure series, the values of the five state variables at the end of subperiod $I, \underline{x}_{k2,e}$, can be transformed back to structure 1 used in subperiod I by the periodicity or transfer matrix $\underline{T}^{-1}$ [Fig. 3]: $\underline{x}_{(k+1)1,s} = \underline{T}^{-1}\underline{x}_{k2,e}$ [see (9)] Now the same structures (structures 1 and 2) and the same state variables are used even in subperiod II as in subperiod I.

$\underline{x}_{(k+1)1,s}$ provides the initial condition of the state variables in structure 1 for subperiod II. The result of the back transformation is $(V_i/2 = 1; t = t_{k+1})$

$$\begin{aligned} \underline{x}_{(k+1)1,s} &= [v_{\rm op} \quad v_{\rm on} \quad v_c \quad Z \cdot i_{\rm op} \quad Z \cdot i_{\rm on}]^T = \underline{T}^{-1} \\ \underline{x}_{k2,e} &= [v_{on} \quad v_{\rm op} \quad -v_c \quad Z \cdot i_{\rm on} \quad Z \cdot i_{\rm op}]^T \end{aligned} \tag{37}$$

where in the first bracket suffix $(k+1)1, s$ and in the second bracket suffix $k2, e$ are omitted. The message of (37) is as follows. At the start of subperiod II, the value of $i_{\rm on}$ takes the

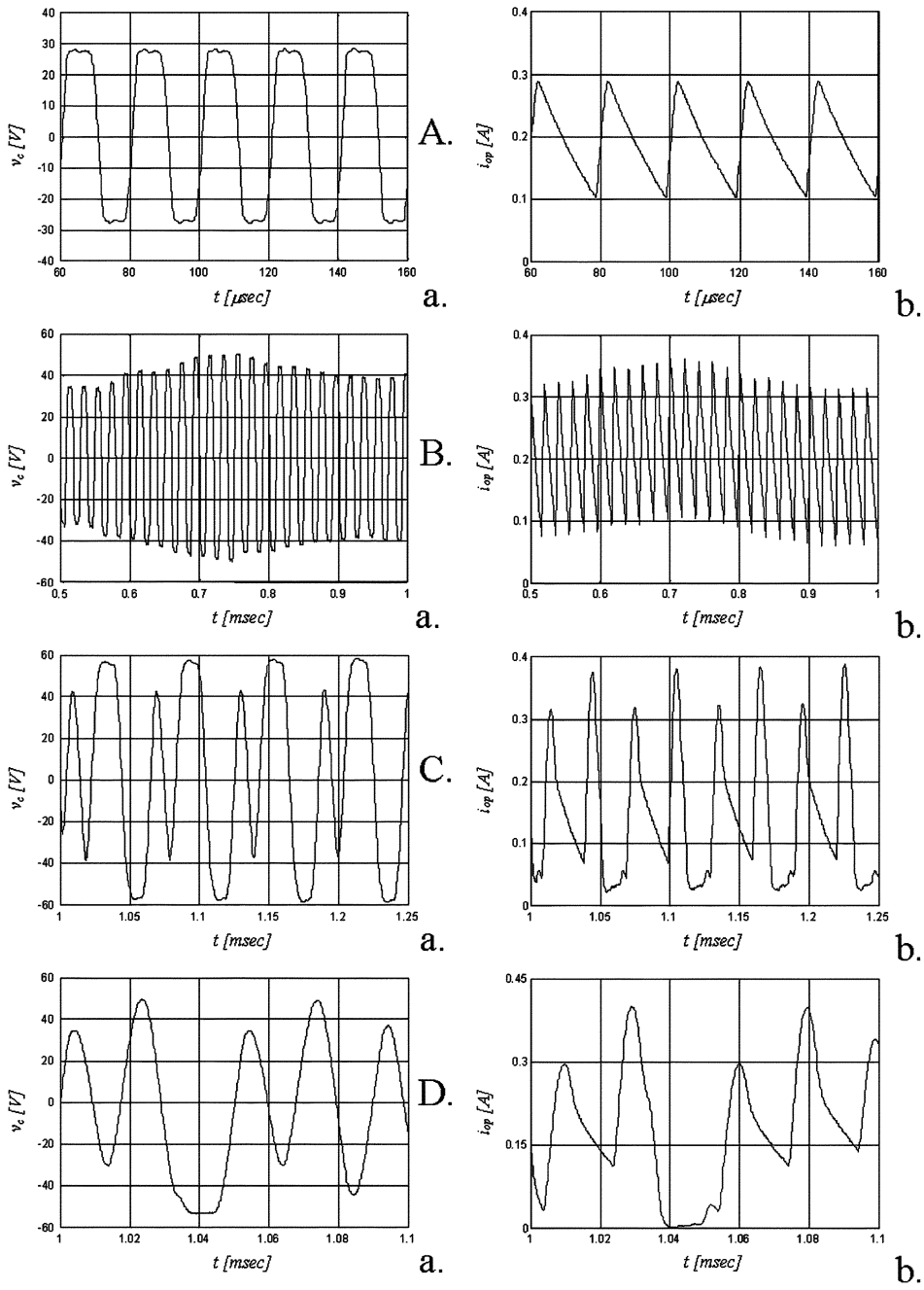

Fig. 11. Oscilloscope trace of (a) the condenser voltage and (b) choke current. (A) Period-1 operation, $K_v = 3$. (B) Quasi-periodic operation, $K_v = 8$. (C) Period-2 operation, $K_v = 13$. (D) Chaotic operation, $K_v = 35$.

value belonging to $i_{\rm op}$ at the end of subperiod I (Fig. 7), that is, $i_{{\rm on}(k+1)1,s} = i_{{\rm op}k2,e}$. Similar statements hold for the other four state variables. We use the same configuration, equations, and state variables in subperiod II as we used in subperiod I but now $v_{\rm op}, v_{\rm on}, v_c, i_{\rm op}$, and $i_{\rm on}$ represent the state variables $v_{\rm on}, v_{\rm op}, -v_c, i_{\rm on}$, and $i_{\rm op}$.

The output voltages and currents are exchanged and the sign of v_c is changed in (37). This result can easily be understood from the periodicity of the time functions and from the operation showing that the corresponding time functions in the two channels are the same only they are shifted by $T_s/2$ to each other. (Fig. 7.) (See the periodicity matrix (A6) in the Appendix.)

VII. Results of Stability Analysis of Feedback-Controlled Resonant DC–DC Converter

A. Simulation and Calculation Results

Simulations performed in the MATLAB and Simulink environments revealed the complex behavior of the feedback-controlled converter as a result of the variation of the proportional gain K_v [Fig. 1(a)]. Similar but other results were presented in [13] and [25] for the converter at different loads. An overall picture of this behavior is offered by the bifurcation diagram (Fig. 8), which shows the various states and the sudden changes or bifurcations of the system due to the variation of bifurcation

parameter K_v. The bifurcation diagram is obtained by sampling the switched condenser voltage of the converter v_c at the start of every switching period in the steady state and plotting these sampled values $v_{ck} = v_c(kT_s)$ as a function of the bifurcation parameter K_v. The data used are as follows: $L = 125$ μH; $C =$ 100 nF; $C_p = C_n = 100$ μF; $R = 6$ Ω; $V_{ip} = -V_{\rm in} = 8$ V; $V_{\rm ref} = 6$ V; $V_L = -6$ V; $V_U = 6$ V. All states have been calculated from the neighboring previous state instead of starting the system from zero initial conditions. On the left side of the bifurcation diagram, there is just one single sampled value $v_{ck} = v_c(kT_s)$ for a given gain K_v, i.e., the condenser voltage v_c repeats itself in each switching period T_s and this corresponds to the stable period-1 range (Fig. 8). By increasing K_v, the first bifurcation takes place between $K_v = 3$ and 4, and it was analyzed with the stability study just presented. However, only the first bifurcation was analyzed in the present paper. Figs. 8, 10, and 11 show further bifurcations and system states contributing significant information about the system behavior in the range of higher K_v values.

Fig. 9 shows the loci of the eigenvalues for the following values of the controller gain: $K_v = 3$ (indicated by +), $K_v = 3.49$ (indicated by o), and $K_v = 4$ (indicated by x). The stable periodic steady-state solution (all of the eigenvalues lie inside the unit circle) loses stability as the controller gain is increased and generate a quasi-periodic solution, since a complex-conjugate pair of eigenvalues passes through the unit circle at $K_v = 3.49$. The eigenvalues were calculated by using the expression of the Jacobian matrix in (27). The pair of eigenvalues at the unit circle is $(0.9296 \pm j0.3698)$. Note that there are altogether five eigenvalues corresponding to the five energy storage components.

The stroboscopic map of the feedback-controlled converter shows the sequence of discrete samples of its arbitrary two state variables taken once in every switching cycle at the T_s interval in the steady state and plotted in the plane of the two variables. Fig. 10 presents the stroboscopic map in quasi-periodic operation [Fig. 10(a), $K_v = 8$], in subharmonic operation in period-8 [Fig. 10(b), $K_v = 23$], and in chaotic operation [Fig. 10(c), $K_v = 35$] in the plane of condenser voltage $v_{ck} = v_c(kT_s)$ versus output voltage $v_{ok} = v_o(kT_s)$. Quasi-periodic operation appears like a closed curve, subharmonic operation is represented by eight points, whereas ten chaotic state appears as a set of organized points, reflecting a multilayered structure and order.

B. Test Results

Tests were performed in order to verify the complex dynamical behavior revealed by computer simulations and stability study. The presentation includes oscilloscope traces of the condenser voltage v_c and choke current $i_{\rm op}$, for the parameter values specified at the beginning of Section VII. The time function of period-1 operation [Fig. 11(A), $K_v = 3$], the quasi-periodic operation [Fig. 11(B), $K_v = 8$], the subharmonic (period-2) operation [Fig. 11(C), $K_v = 13$] and the chaotic operation [Fig. 11(D), $K_v = 35$] are presented. Qualitatively, the measurement results are in good agreement with the simulation ones. Quantitatively, there are deviations due to the presence of parasitic elements in the practical circuit (ideal components were assumed in simulations and in the stability analysis). These discrepancies do not influence the detected phenomena; they only shift the bifurcation points (e.g., the Hopf bifurcation in the experimental circuit occurs at a higher controller gain, about $K_v = 7$).

VIII. Conclusion

The paper applied conventional tools for the stability analysis of variable-structure piecewise-linear nonlinear feedback systems, namely, the eigenvalues of the Jacobian matrix of the PMF belonging to a fixed point of the system. The paper introduced two contributions; the first one is less significant, while the second one is the major contribution. First, it utilized the periodicity of the variable structure and this way it permits the application of the same equations written only for one part of the entire configuration which is continuously repeated after switching actions.

Second, and most important, it determined the Jacobian matrix by using the small differences of the state vectors compared to their steady-state values at the start and end of subperiods and at the switching instant. There was no need to determine the derivatives of the PMF at the fixed point. The Jacobian matrix was obtained directly from the relations among the small differences of the state vectors. In addition, all steps were interpreted graphically in Figs. 3 and 4. Consequently, this method offered an alternative way to derive the Jacobian matrix or, which is more significant, a simpler and faster way to determine it. The key element of this method was the introduction of the auxiliary state vector for preserving constant switching instants for the switchings depending on state variables even after the small excursion of the state variables from the steady state, although in reality it varies a small extent.

In addition, the application of the method was presented in the example of a feedback-controlled resonant dc–dc converter. Simulations, calculations, and test results illustrated the theoretical considerations.

Appendix
Derivation of State Equations

The linear state equations of the structures in subperiod I are as follows (Figs. 5 and 6). For structure 1, we have

$$\frac{d\underline{x}^*}{dt} = \underline{A}_1^* \cdot \underline{x}^* + \underline{B}_1^* \tag{A1}$$

where

$$A_1^* = \begin{bmatrix} -1/R_pC_p & 0 & 0 & 1/C_p & 0 \\ 0 & -1/R_nC_n & 0 & 0 & 1/C_n \\ 0 & 0 & 0 & 1/C & 0 \\ -1/L_p & 0 & -1/L_p & 0 & 0 \\ 0 & -1/L_n & 0 & 0 & 0 \end{bmatrix}$$

$$B_1^* = [0 \quad 0 \quad 0 \quad 1/L_p \quad 0]^T$$

$$\underline{x}^* = [v_{\rm op} \quad v_{\rm on} \quad v_c \quad i_{\rm op} \quad i_{\rm on}]^T.$$

Rewriting (A1) in per unit ($L_p = L_n = L; C_o = C_p = C_n = C; R_p = R_n = R$), we have

$$\frac{d\underline{x}}{dt_r} = \underline{A}_1 \cdot \underline{x} + \underline{B}_1 \tag{A2}$$

where

$$\underline{A}_1 = \begin{bmatrix} -a & 0 & 0 & b & 0 \\ 0 & -a & 0 & 0 & b \\ 0 & 0 & 0 & \pi & 0 \\ -\pi & 0 & -\pi & 0 & 0 \\ 0 & -\pi & 0 & 0 & 0 \end{bmatrix}$$

$$\underline{B}_1 = \begin{bmatrix} 0 \\ 0 \\ 0 \\ \pi \\ 0 \end{bmatrix} \qquad \underline{x} = \begin{bmatrix} x_1 \\ x_2 \\ x_3 \\ x_4 \\ x_5 \end{bmatrix}$$

and

$$\begin{aligned} x_1 &= \frac{v_{\rm op}}{V_i/2} \\ x_2 &= \frac{v_{\rm on}}{V_i/2} \\ x_3 &= \frac{v_c}{V_i/2} \\ x_4 &= \frac{Z \cdot i_{\rm op}}{V_i/2} \\ x_5 &= \frac{Z \cdot i_{\rm on}}{V_i/2} \\ t_r &= \frac{t}{T_r} \\ V_i/2 &= V_{ip} = V_{\rm in} \\ T_r &= T_s/2 = \pi\sqrt{LC} \\ a &= \frac{T_r}{T_o} \\ b &= \frac{\pi T_c}{T_o} = \frac{\pi C}{C_o} \\ T_o &= RC_o \\ T_c &= RC \\ Z &= \sqrt{L/C}. \end{aligned}$$

For structure 2, we have

$$\frac{d\underline{x}^*}{dt} = \underline{A}_2^* \underline{x}^* \tag{A3}$$

where

$$\underline{A}_2^* = \begin{bmatrix} -1/R_pC_p & 0 & 0 & 1/C_p & 0 \\ 0 & -1/R_nC_n & 0 & 0 & 1/C_n \\ 0 & 0 & 0 & 0 & 0 \\ 0 & 0 & 0 & -1/L_p & 0 \\ 0 & 0 & 0 & 0 & -1/L_n \end{bmatrix}.$$

Rewriting (A3) in per unit yields

$$\dot{\underline{x}} = \underline{A}_2 \cdot \underline{x}$$

$$\underline{x} = \begin{bmatrix} x_1 \\ x_2 \\ x_3 \\ x_4 \\ x_5 \end{bmatrix}$$

$$\underline{A}_2 = \begin{bmatrix} -a & 0 & 0 & b & 0 \\ 0 & -a & 0 & 0 & b \\ 0 & 0 & 0 & 0 & 0 \\ -\pi & 0 & 0 & 0 & 0 \\ 0 & -\pi & 0 & 0 & 0 \end{bmatrix}. \tag{A4}$$

Utilizing the symmetry and periodicity of the converter on the basis of Figs. 6 and 7, the transfer matrix is

$$\underline{T} = \underline{T}^{-1} = \begin{bmatrix} 0 & 1 & 0 & 0 & 0 \\ 1 & 0 & 0 & 0 & 0 \\ 0 & 0 & -1 & 0 & 0 \\ 0 & 0 & 0 & 0 & 1 \\ 0 & 0 & 0 & 1 & 0 \end{bmatrix}. \tag{A5}$$

ACKNOWLEDGMENT

The authors would like to thank the Hungarian-Romanian Intergovernmental S & T Cooperation Programme and the HAS and Japanese Society for the Promotion of Science (JSPS) for the support stemming from their cooperation.

REFERENCES

[1] S. Banerjee and G. C. Verghese, *Nonlinear Phenomena in Power Electronics*. Piscataway, NJ: IEEE Press, 2001.

[2] J. Guckenheimer and P. Holmes, *Nonlinear Oscillations, Dynamical Systems, and Bifurcations of Vector Fields*. New York: Springer-Verlag, 1992.

[3] R. C. Hilborn, *Chaos and Nonlinear Dynamics*. New York: Oxford Univ. Press, 1994.

[4] F. C. Moon, *Chaotic and Fractal Dynamics*. New York: Wiley, 1992.

[5] E. Ott, *Chaos in Dynamical Systems*. Cambridge, U.K.: Cambridge Univ. Press, 1997.

[6] M. A. Aizerman and F. R. Gantmakher, "Stability in the linear approximation of the periodic solution of a system of differential equations with discontinuous right-hand part" (in Russian), *Prikl. Mat. Mekh.*, vol. 21, pp. 658–669, 1957.

[7] A. F. Filippov, *Differential Equations with Discontinuous Right-Hand Sides*. Dordrecht, The Netherlands: Kluwer, 1988.

[8] V. S. Baushev *et al.*, "Local stability of periodic solutions in sample data control systems," in *Automation and Remote Control*. New York: Plenum, 1992, pt. 2, vol. 53, pp. 865–871.

[9] Zh. T. Zhusubaliyev and E. Mosekilde, *Bifurcations and Chaos in Piecewise-Smooth Dynamical Systems*, Singapore: World Scientific, 2003.

[10] L. Benadero *et al.*, "Two-dimensional bifurcation diagrams. Background pattern of fundamental DC-DC converters with PWM control," *Int. J. Bifurc. Chaos*, vol. 13, pp. 427–451, 2003.

[11] A. El Aroudi and R. Leyva, "Quasiperiodic route to chaos in a PWM voltage-controlled DC-DC boost converter," *IEEE Trans. Circuits Syst. I*, vol. 48, no. 8, pp. 967–978, Aug. 2001.

[12] Y. Kuroe, "Computer algorithm to analyze stability of power electronic systems," in *Proc. Power Conversion Conf.*, Osaka, Japan, Apr. 2–5, 2002, pp. 293–298.

[13] O. Dranga *et al.*, "Stability analysis of a feedback controlled resonant DC-DC converter," *IEEE Trans. Ind. Electron.*, vol. 50, no. 1, pp. 141–152, Feb. 2003.

[14] H. H. C. Iu and C. K. Tse, "Bifurcation behavior of parallel-connected buck converters," *IEEE Trans. Circuits Syst.*, vol. 48, no. 2, pp. 233–240, Feb. 2001.

[15] L. Benadero *et al.*, "Bifurcations analysis in PWM regulated DC-DC converters using averaged models," in *Proc. EPE-PEMC'02*, Croatia, 2002, Available: [CDRom].

[16] O. Woywode and H. Güldner, "Application of statistical analysis to DC-DC converters," in *Proc. Int. Power Electron. Conf., IPEC 2000*, Tokyo, Japan, Apr. 2000, pp. 90–94.

[17] C.-C. Fang, "Exact orbital stability analysis of static and dynamic Ramp compensations in DC-DC converters," in *Proc. ISIE'2001 Conf.*, vol. III, Pusan, Korea, 2001, pp. 2124–2129.

[18] A. El Aroudi *et al.*, "Quasiperiodic route to chaos in DC-DC switching regulators," in *Proc. ISIE'2001 Conf.*, vol. III, Pusan, Korea, pp. 2130–2135.

[19] J. L. R. Marrero *et al.*, "Analysis of the chaotic regime for dc-dc converters under current mode control," in *Proc. IEEE Power Electron. Specialists Conf.*, 1996, pp. 1477–1483.

[20] D. Carton *et al.*, "Self-similarity and chaos in a current mode PWM-bridge," in *Proc. 6th Int. Conf. Electrimacs 99*, vol. I, Lisboa, Portugal, Sept. 14–16, 1999, pp. 109–114.

[21] W. C. Y. Chan and C. K. Tse, "Study of bifurcations in current-programmed DC-DC boost converters: From quasiperiodicity to period doubling," *IEEE Trans. Circuits Syst. I*, vol. 44, no. 12, pp. 1129–1142, Dec. 1997.

[22] J. H. Chen *et al.*, "Experimental stabilization of chaos in a voltage-mode DC drive system," *IEEE Trans. Circuits Syst. I*, vol. 47, no. Jul., pp. 1093–1095, 2000.

[23] I. Rácz, "Calculation of thyristor controlled electric machines with matrix calculus," in *Proc. 1st Conf. Power Electron. Motion Control, PEMC'70*, Budapest, Hungary, 1970, pp. 2.1.1–2.1.11.

[24] M. Orabi and T. Ninomiya, "Analysis of PFC converter stability using energy balance theory," in *Proc. IECON'03*. Roanoke, VA, 2003, pp. 544–549.

[25] O. Dranga and I. Nagy, "Stability analysis of feedback controlled resonant DC-DC converter using poincare map function," in *Proc. ISIE*, vol. III, Pusan, Korea, Jun. 12–16, 2001, pp. 2142–2147.

[26] J. Hamar and I. Nagy, "Asymmetrical operation of dual channel resonant DC-DC converters," *IEEE Trans. Power Electron.*, vol. 18, no. 1, pp. 83–94, Jan. 2003.

Octavian Dranga was born in Romania in 1971. He received the B.Sc., M.Sc., and Ph.D. degrees in control engineering from the "Politechnica" University of Timiooara, Timiooara, Romania in 1995, 1996, and 2001, respectively.

He was with the "Politehnica" University of Timiooara from 1996 to 1998. During 1998–2001, he was a Ph.D. student at the Budapest University of Technology and Economics, Budapest, Hungary. He held postdoctoral research positions with Hong Kong Polytechnic University (2001–2002), University of Hull, Hull, U.K. (2003), and Utsunomiya University, Tochigi, Japan (2003–2004). He is currently with the Hong Kong Polytechnic University as a Research Fellow. His research interest is in the study of nonlinear phenomena in power electronics. He has authored 40 papers.

Balázs Buti was born in Berettyóújfalu, Hungary, in 1978. He received the M.Sc. degree from the Budapest University of Technology and Economics, Budapest, Hungary, in 2001, where he is currently working toward the Ph.D. degree.

His research interests focus on power electronics, nonlinear systems, and control systems. He is the coauthor of 15 technical papers.

István Nagy (M'92–SM'99–F'00) received the Ph.D. degree from the Technical University of Budapest, Budapest, Hungary, in 1960.

He has been associated with the Institute of Automation and Computation, Hungarian Academy of Sciences, Budapest, since 1960, where he headed the Department of Power Electronics for 15 years. He became a Full Professor with the Technical University of Budapest, Budapest, Hungary, in 1975. He was a Visiting Professor at universities in Sweden, Germany, India, New Zealand, Italy, Canada, the U.S., and Japan. His research interests are power electronics, control of ac drives, and nonlinear dynamics. He has authored or coauthored 13 textbooks and approximately 170 technical papers and holds 13 patents.

Prof. Nagy is a member of the Hungarian Academy of Sciences, chairman of EPE-PEMC council, member of the Hungarian IEE and EPE. He is also a member of AdCom of the IES and the IEEE Power Electron Society.

Hirohito Funato (S'93–M'95) was born in Fukushima, Japan, in 1964. He received the B.Eng., M.Eng., and Ph.D. degrees in electrical engineering from Yokohama National University, Yokohama, Japan, in 1987, 1989, and 1995, respectively.

From 1989 to 1991, he was with Tokyo Electric Power Company, Inc. In 1995, he joined Utsunomiya University, Tochigi, Japan, as a Research Associate, where he is currently an Associate Professor with the Department of Electrical and Electronics Engineering. His research interests include digital control of power electronics circuits, power electronics in power systems, and renewable energy.